# Dispersions of Polymer-Modified Carbon Nanotubes: A Small-Angle Scattering Investigation

Anastasia A. Golosova,[†,‡] Joseph Adelsberger,[†] Alessandro Sepe,[†] Martin A. Niedermeier,[†] Peter Lindner,[§] Sergio S. Funari,[∥] Rainer Jordan,[‡,⊥] and Christine M. Papadakis*,[†]

[†]Physikdepartment, Technische Universität München, Fachgebiet Physik weicher Materie/Lehrstuhl für Funktionelle Materialien, James-Franck-Straße 1, 85747 Garching, Germany
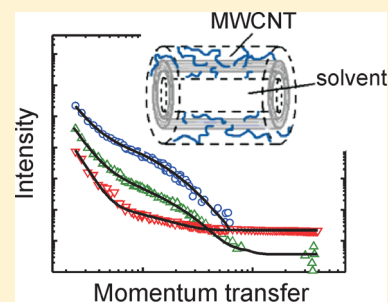
[‡]Wacker-Lehrstuhl für Makromolekulare Chemie, Department Chemie, Technische Universität München, Lichtenbergstraße 4, 85747 Garching, Germany

[§]Institut Laue-Langevin, BP 156, 6, rue Jules Horowitz, 38042 Grenoble, France

[∥]HASYLAB at DESY, Notkestraße 85, 22607 Hamburg, Germany

[⊥]Professur für Makromolekulare Chemie, Department Chemie, Technische Universität Dresden, Zellescher Weg 19, 01069 Dresden, Germany

**ABSTRACT:** Carbon nanotubes (CNTs) were modified with polystyrene (PS) using self-initiated photografting photopolymerization. In order to optimize their utilization in CNT/polymer nanocomposites, a thorough characterization of their dispersions in solvents is of key importance. Using small-angle scattering, we have studied the effect of the modification on the agglomeration behavior in dilute toluene dispersions. Whereas small-angle X-ray scattering gives overall information, small-angle neutron scattering together with the use of deuterated solvents highlights the polymer shells or the CNTs. The structure of the CNTs and their agglomerates were modeled as fractal aggregates of homogeneous or core−shell cylinders for single- and multiwalled CNTs, respectively. In this way, we have characterized the dispersibility of the CNTs as well as the thickness of the shell formed by the grafted polymers in dependence on the time of polymerization.

## INTRODUCTION

CNTs are synthetic allotropes of carbon. The main feature that makes CNTs exceptional in the row of the other carbon forms (carbon black, graphite, diamond, and fullerenes) is their cylindrical structure with a very high aspect ratio (up to 1000), which allows us to consider them as 1D objects. The honeycomb lattice structure of CNTs, where the sp$^2$ hybridized carbon atoms are connected to each other by $\sigma$ and $\pi$ bonding, leads to impressive mechanical and electrical properties.[1] For instance, their tensile strength is with 10−500 GPa much higher than the one of high-strength steel (2 GPa), their elastic modulus is comparable to the one of diamond (ca. 1 TPa), and the electric current-carrying capability of CNTs is estimated to be ca. $1 \times 10^9$ A/cm$^2$, which is 3 orders of magnitude higher than the one of copper. Moreover, CNTs are thermally stable up to 2800 °C in vacuum and up to 750 °C in air and exhibit high thermal conductivity. Also, the hollow structure of the CNTs makes them very light, with a bulk density of ca. 0.15 g/cm$^3$ and a solid density of about 1.30−1.70 g/cm$^3$, which is half the density of aluminum.

Apart from an early report from 1952,[2] CNTs have been known since the early 1990s.[3] Still, many aspects have not been clarified. For instance, there is still a lack of knowledge about the agglomeration behavior of CNTs in dispersions. For the visualization of CNTs and their agglomerates, microscopic techniques like atomic force microscopy (AFM), scanning and transmission electron microscopy (SEM and TEM),[4−6] and even optical bright-field and dark-field microscopy[7] have been used. However, the microscopic observation may not in all cases reflect the real behavior of the CNTs: Both, the sample preparation by drop-casting or spin-coating from very dilute dispersion onto a substrate and the solvent evaporation and the interaction of the CNTs with the substrate surface, may have a significant influence on the arrangement of CNTs and may falsify the observations.

At the same time, characterization of the agglomerates directly in dispersion is highly desirable, since one of the main pathways to prepare CNT/polymer nanocomposites is solution processing; that is, both components are separately dissolved in a common solvent, followed by comixing and solution casting.[8−10] The dispersion of CNTs in solvent is in itself challenging because CNTs do not easily deagglomerate as their extended $\pi$-electron system in the tube walls leads to an effective van der Waals attraction between them.[11] This attraction together with hydrophobicity and the chemically smooth surface of the CNTs result in the formation of large agglomerates which behave differently from individually separated CNTs.[11,12] As a consequence, the electrical, thermal, and mechanical properties of the final nanocomposite depend

strongly on the agglomeration state of the CNTs in dispersion. For instance, CNT/epoxy nanocomposites containing poorly dispersed CNTs exhibited higher storage and loss moduli and a more complex viscosity behavior than the ones obtained from well-dispersed CNTs.[12] On the contrary, an improved tensile strength and a higher elongation at break were found by the same authors for the case of well-dispersed CNTs along with much higher electrical and thermal conductivity; that is, the well-dispersed CNTs provide conductive paths efficiently even at low CNT content. Thus, the quality of the dispersion in terms of its stability and the degree of deagglomeration has a strong impact on the properties of the final nanocomposite and requires a thorough investigation.

To overcome the problem of aggregation, both chemical and physical modification of CNTs have been widely envisaged.[13] However, it is quite challenging to develop methods to tune the surface properties of CNTs for their further application in nanocomposites. For instance, though the presence of surfactants stabilizes aqueous dispersions of CNTs for several weeks and even months,[14] the resulting double dielectric layer around the CNTs hinders the conduction of electrical current between them. The dispersion of CNTs by physical adsorption of polymers is promising because it improves the compatibility with the matrix and preserves the CNTs' properties. However, the adhesive energy between the physically adsorbed polymers and the CNTs may not be sufficiently high to transfer the stress between them efficiently,[15] resulting in pulling-out of CNTs from the matrix during deformation of the nanocomposite.[16,17]

Therefore, modification of CNTs by means of covalent grafting of polymer chains to the CNTs' framework is the method of choice for improving the dispersion ability of the CNTs in view of their introduction into the polymer matrix, since (i) the covalently bound grafts on the CNTs' walls cannot be easily removed, e.g. by deformation, and (ii) long grafted polymer chains serve as perfect bridges between the CNTs and polymer matrix and improve the load transfer between matrix and CNTs.

In our previous work, we developed an easy yet efficient protocol for the covalent modification of the CNTs with polystyrene (PS) grafts:[18] The self-initiated photografting photopolymerization (SIPGP) allows regulating the grafting density and the morphology of the PS grafts, i.e., the length and the branching, by variation of the polymerization time.[19] Here, we investigate these PS-modified CNTs in dilute (0.5 and 1.0 mg/mL) toluene dispersion, which is a good solvent for PS, focusing on the dispersion ability of single- (SW) and multiwalled (MW) CNTs in dependence on the polymerization time. Small-angle neutron scattering (SANS) covering a large range of momentum transfers revealed structural information on a large range of length scales. Moreover, contrast variation was carried out by using fully deuterated toluene (D-toluene) or a mixture of protonated toluene (H-toluene) and D-toluene and allowed us to highlight either the polymer shell or the CNTs. Additional small-angle X-ray scattering (SAXS) on dispersions of the CNTs in H-toluene gave combined information and verified the results from SANS.

SAXS and SANS have previously been applied for probing CNT dispersions.[11,20−22] For nearly one-dimensional CNTs as isolated, randomly distributed, long, rod-like particles, the scattering intensity is expected to follow a power law, $I(q) \propto q^{\alpha}$, where $q$ is the magnitude of the scattering vector and the exponent $\alpha$ is $-1$.[23] Such a behavior was observed in very dilute dispersions of CNTs and at a high concentration of dispersing agent, e.g., at a concentration of SWCNTs of 0.02 wt. % and a surfactant (sodium dodecylbenzene sulfonate)/SWCNT ratio of 10:1.[11] In most other works, values of $\alpha$ between $-2.5$ and $-3$ were observed, which was attributed to the aggregation of the CNTs.

Modeling of the full scattering curves of CNTs in dispersion has only been attempted in very few studies,[24,25] and mainly for the case of CNTs dispersed in the polymer matrix. Zhao et al. used ultrasmall angle X-ray scattering (USAXS) to study the morphology of nanocomposites from polyamide 6 and CNTs prepared by in situ polymerization of $\varepsilon$-caprolactam in the presence of pristine or carboxylated multiwalled CNTs.[24] The USAXS curves taken at a MWCNT concentration of 0.1 wt. % did not follow the power law with $\alpha = -1$. Neither could they be fitted by the stiff-rod model, which is a simplified rigid-rod model for single polydisperse cylinders. On the contrary, a model based on fractal ordering of short rod-like segments having a diameter of ca. 300 Å and a length of ca. 800 Å matched the scattering curves well. Thus, the CNTs have a wormlike rod conformation; however, the authors noted that the same model can as well be attributed to agglomerates of straight rods having a fractal correlation.

Several years later, Zhao et al. suggested a simplified tube form factor.[24] It differs from the previously described ones, exact rod form factor or stiff rod form factor, mainly in the intermediate $q$ range which is due to the two-dimensional character of the tube wall. Still, the fits were not perfect, even at very low concentrations of CNTs (0.01 wt. %). At higher concentrations, when agglomerates of the CNTs are present, the authors accounted for the long-range correlations by a fractal structure factor.

In the present work, the experimental SANS and SAXS curves of the CNT dispersions are modeled using the form factor of homogeneous or core−shell cylinders for SW or MWCNTs, respectively. A fractal structure factor is used to model their correlation. In this way, we describe both the structure and dispersion ability of the SW and MWCNTs depending on the polymerization time. The broad distribution of the CNTs' dimensions is taken into account by including polydispersity of the cylinder diameter into the models. The probably present length distribution was not taken into account to keep the number of parameters as low as possible.

This paper is structured as follows: After describing the initial characterization of the modified CNTs by TGA, we present an overview of the SANS and SAXS experiments and the obtained curves and introduce the models used for fitting the experimental data. Then, the fitting results on the structure of the CNTs as well as the dependence of their dispersion ability on the amount of grafted polymer (i.e., the polymerization time) are presented. Finally, the results are discussed and compared to previous results from the literature.

## ■ EXPERIMENTAL SECTION

**Materials.** MWCNTs (Baytubes) with 3−15 walls, having inner and outer diameters of ca. 40 and 100−160 Å, respectively, and lengths of ca. 1−10 $\mu$m, were provided by Bayer AG (Leverkusen, Germany). SWCNTs were obtained from BuckyUSA, TX, U.S.A., and have a diameter of 7−25 Å. Both SW and MWCNTs were functionalized with PS grafts using surface-initiated photografting and photopolymerization (SIPGP) as follows. An amount of 4 mg of CNTS was added to ca. 8 mL of freshly distilled styrene in a glass photoreaction vial charged with a magnetic stirrer. After the reaction mixture was

degassed by three freeze−thaw cycles, it was ultrasonicated for 5 min to disperse the CNTS in the monomer. Polymerization was performed at room temperature for different time periods (1 or 3 days) by irradiation with UV ($\lambda_{max}$ = 350 nm) and under constant intensive stirring. After the polymerization, the reaction mixture was diluted with toluene, a good solvent for PS, and was ultasonicated for 5−10 min to remove nongrafted PS from the CNT surface. The dispersion was pressure filtered through Teflon filters (0.45 $\mu$m) and thoroughly washed with an excess of toluene (4−6 portions of ca. 50 mL). The filtrate was collected and vacuum-dried to remove the solvent. Details on the reaction mechanism will be published in ref 18. Here, we investigated native CNTs as well as CNTs with PS grafts obtained after 1 or 3 days of polymerization (denoted SW(MW)CNT-PS-1d or SW(MW)CNT-PS-3d, respectively). HPLC-grade toluene, $C_7H_8$ (H-toluene), from Sigma-Aldrich, Steinheim/München, Germany and fully deuterated toluene ($C_7D_8$, denoted D-toluene) from Deutero GmbH (Kastellaun, Germany) were used.

The solid densities of MW and SWCNTs are ca. 1.4 and ca. 1.5 g/cm$^3$, respectively, and the mass density of PS $\rho_{PS}$ = 1.05 g/cm$^3$.

The PS weight fractions in the PS-modified CNTs were determined by thermogravimetric analysis (TGA) in dependence on the polymerization time.[18] The measurements were performed under an inert nitrogen atmosphere with a flow of 200 mL/min. The temperature was increased from 35 to 800 °C with a rate of 10 K/min.

**Small-Angle X-ray Scattering (SAXS).** SAXS experiments were carried out at beamline A2 at HASYLAB at DESY in Hamburg, Germany. An X-ray wavelength of 1.50 Å and a sample-to-detector distance of 1.30 m were used, resulting in a q range of 0.022−0.30 Å$^{-1}$. A MarCCD area detector was used for the detection of the scattered intensity. The pixel size was 158 $\mu$m × 158 $\mu$m. A beamstop carrying a photodiode blocked the direct beam and served for measurement of the sample transmission. Dispersions of CNTs (SWCNT, MWCNT, SWCNT-PS-1d, MWCNT-PS-1d, SWCNT-PS-3d, and MWCNT-PS-3d) in protonated toluene ($C_7H_8$, H-toluene) with CNT concentrations of 1 mg/mL were prepared by 15 min of ultrasonication right before the measurements. The dispersions were filled into glass capillaries with 1 mm path length, and SAXS data were collected at room temperature with a measuring time of 420 s. The raw data were corrected for dark current and background scattering from the empty cell and solvent using the Fit2D software. Azimuthal averaging was also performed using Fit2D. The q calibration was carried out using collagen (rat tendon tail). The coherent X-ray scattering length densities (SLD) of H-toluene, PS, and CNTs are 8.0 × 10$^{-6}$, 9.6 × 10$^{-6}$, and 12 × 10$^{-6}$ Å$^{-2}$, respectively,[26] as determined from the mass densities of toluene, PS, SWCNTs, and MWCNTs which are 0.87, 1.05, 1.3−1.5, and 1.5−1.7 g/cm$^3$, respectively.

**Small-Angle Neutron Scattering (SANS).** SANS experiments on the CNT dispersions were performed at the instrument D11 at ILL (Grenoble, France).[27,28] Dispersions of native SWCNTs and MWCNTs as well as SW(MW)CNT-PS-1d and SW(MW)CNT-PS-3d were prepared by ultrasonication in toluene for 15 min before the injection into a Hellma quartz cell (QS-110 with a path length of 1 mm) and then measured at room temperature. The concentration of the CNTs was 0.5 or 1 mg/mL in fully deuterated toluene ($C_7D_8$, D-toluene) or in the mixture $C_7H_8$/$C_7D_8$ = 89/11 vol. % (HD-

toluene). In this way, the polymer shell or the bare CNTs were highlighted. The coherent neutron SLDs (SLD) of D-toluene, HD-toluene, PS, and CNTs are 5.66 × 10$^{-6}$, 1.40 × 10$^{-6}$, 1.44 × 10$^{-6}$, and 4.7−5.7 × 10$^{-6}$ Å$^{-2}$, respectively.[29] The experiments were carried out at sample-to-detector distances of 1.2, 8, and 20 m and a neutron wavelength of 8 Å, resulting in a q range of 0.00243−0.4 Å$^{-1}$. The wavelength spread $\Delta\lambda/\lambda$ was 9%. SANS images were taken with accumulation times between 300 and 7200 s, depending on the sample and sample-to-detector distance. Azimuthal averaging, background correction and normalization with a 1 mm water sample were done with standard data treatment procedures in order to yield the differential scattering cross sections in absolute units of [1/cm].[30]

## ■ RESULTS

SIPGP was used to modify SW and MWCNTs by PS in various amounts. TGA confirms that this process is successful. Table 1

**Table 1. Weight Fraction of PS in Modified SW(MW)CNTs as Determined by TGA**

|  | wt. fraction (%) | |
| --- | --- | --- |
|  | CNT-PS-1d | CNT-PS-3d |
| SWCNT | 10 ± 1 | 18 ± 1 |
| MWCNT | 16 ± 1 | 32 ± 1 |

shows that the weight fraction of PS varies between 10 and 32 wt. %. It is higher for MWCNTs than for SWCNTs which may be due to intercalative growth of PS in addition to growth at the surfaces of the MWCNTs. Moreover, both for SWCNTs and MWCNTs, the weight fraction of PS increases with polymerization time, as expected. We thus anticipate that the length of the PS grafts on the CNTs and/or the grafting density increases with polymerization time; however, this cannot be decided from TGA which is an integral method. SAXS and SANS will elucidate this issue.

**Survey of SAXS and SANS Experiments.** In this section, we present an overview of the scattering curves, namely SAXS data of the dispersions of native SW(MW)CNTs and of modified CNTs (SW(MW)CNT-PS-1d and SW(MW)CNT-PS-3d) in H-toluene and SANS data in D- and in HD-toluene (Figure 1).

The first difference between SANS and SAXS is that different q ranges are covered: The SANS curves cover q values from 0.00243 to 0.4 Å$^{-1}$, which results in observable length scales $2\pi/q \cong$ 20−2500 Å; thus, length scales between the CNTs diameter and the long-range correlations between the CNTs in the dispersions are accessible. However, in some cases, the scattered intensity above ca. 0.07 Å$^{-1}$ was below the detection limit; thus, only length scales above 90 Å are accessible. In contrast, the SAXS experiments cover a q range of 0.022−0.30 Å$^{-1}$, which corresponds to length scales of 20−280 Å, and thus give information on the small features of the system, like the CNTs' diameter or the thickness of the polymer shell. Therefore, the results of the SAXS experiments are complementary to the ones from SANS in the high q regime, where the statistics of the SANS data are poor.

The second significant difference arises from the scattering contrast conditions in SANS and SAXS. Whereas in SAXS, both the CNTs and the PS grafts display contrast with the solvent and contribute to the scattering signal, in SANS, the choice of solvent, D-toluene or HD-toluene allows to highlight the PS
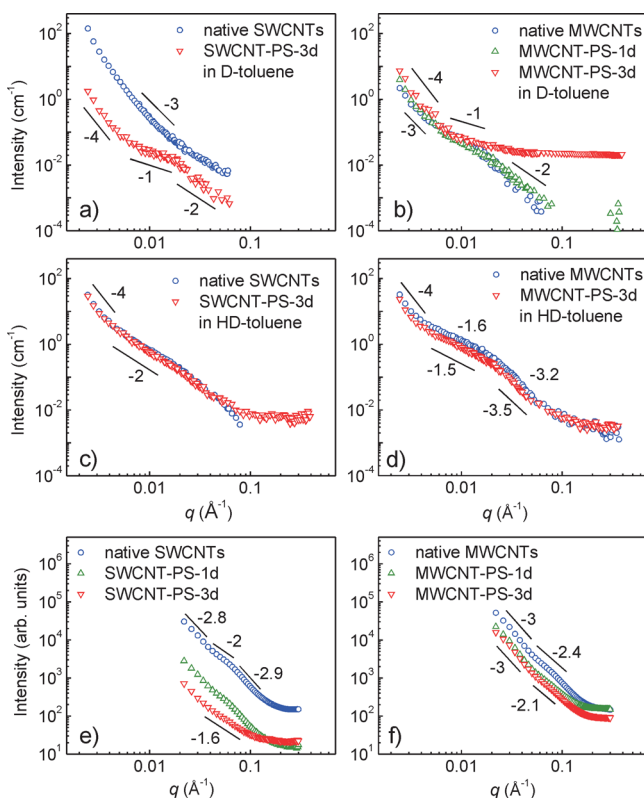
**Figure 1.** SANS curves in D-toluene (a and b) and in HD-toluene (c and d) at 0.5 mg/mL and SAXS curves in H-toluene at 1.0 mg/mL (e and f). In all plots, the lines represent power laws $I(q) \propto q^\alpha$ with the $\alpha$-value given. Uncertainties see Figure 3.



**Figure 2.** Scattering length densities (SLDs) for (a) SAXS in H-toluene and (b) SANS in D- and HD-toluene.

shell (D-toluene) or the CNTs (HD-toluene), respectively (Figure 2).

The SANS curves of native and modified SWCNTs dispersions in D-toluene (Figure 1a) differ significantly from each other: The curve of the non-modified SWCNTs decays almost like $I(q) \propto q^\alpha$ with $\alpha \cong -3$ to $-4$. In contrast, the curve of SWCNT-PS-3d features an intermediate region (0.006 Å$^{-1}$ < $q$ < 0.02 Å$^{-1}$) with $\alpha \cong -1$, as expected for rod-like scatterers. However, strong forward scattering at $q$ < 0.004 Å$^{-1}$ with $\alpha \cong -4$ suggests the presence of large agglomerates of the CNTs in the toluene dispersion, even though they are modified with PS. At high $q$ values, a power-law with $\alpha \cong -2$ is observed, which is presumably due to the surface roughness of the modified CNTs, i.e., the polymer shell. To understand the features in the high $q$ region, the SAXS curves must be considered.

As mentioned above, the SAXS curves describe mainly the small scale features, like the walls of the CNTs and the PS grafts. For native and modified SWCNTs, they display $\alpha \cong -2$ to $-3$ for SWCNTs and SWCNT-PS-1d (Figure 1e), similarly to the SANS profiles in the high $q$ region. For SWCNT-PS-3d, a lower slope, $\alpha = -1.6$, is observed. For perfectly smooth surfaces, $\alpha = -4$ (the Porod's law) has been predicted.[23] However, neither for native nor for modified CNTs, a smooth surface is expected because native CNTs have numerous carbonaceous impurities like carbon black, defects on their carbon networks, and twists which lead to a rough surface. The PS shell leads to a further increase of the roughness. With increasing amount of grafted PS, the intensity at lower $q$ values (below 0.04 Å$^{-1}$) and the slope of the curves decrease. The meaning of these changes will only become clear upon
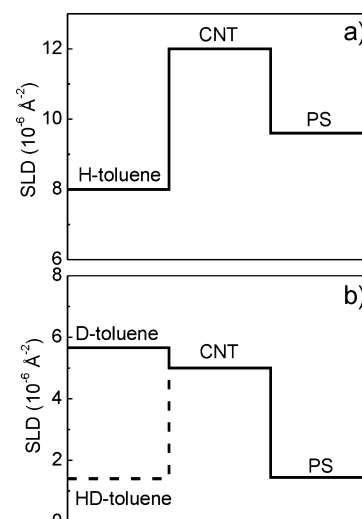
modeling, see below. We note that it is not straightforward to compare these slopes with the ones from SANS in the overlap region 0.02−0.07 Å$^{-1}$ because of the different contrast conditions.

In HD-toluene, where the bare CNTs are highlighted, the difference between the scattering profiles obtained for native SWCNTs and SWCNT-PS-3d is not as pronounced as in the case of dispersions in D-toluene (Figure 1c). However, it will be shown in the following sections that despite the similarities, the real-space structures are different. The slopes are $\alpha \cong -2$ almost for the whole $q$ range, except for $q$ < 0.004 Å$^{-1}$ where intense forward scattering with $\alpha \cong -4$ is observed.

The SANS scattering curves from the dispersions of native and modified MWCNTs in D-toluene are depicted in Figure 1b. As in the case of SWCNTs, the $q$ range can be divided into 3 regions: (i) forward scattering in the low $q$ range ($q$ < 0.006 Å$^{-1}$) with $\alpha \cong -4$, implying again the formation of large agglomerates, (ii) the intermediate region (0.006 Å$^{-1}$ < $q$ < 0.02 Å$^{-1}$) with $\alpha = -2$ to $-1$, and (iii) the high $q$ range ($q$ > 0.02 Å$^{-1}$). The latter show the following characteristics: (ii) Unlike in the case of SWCNTs, where we observed a significant difference in scattering profiles for native and modified samples, native MWCNTs dispersed in D-toluene also exhibit a small region with $\alpha$ close to $-1$ ($\alpha \cong -1.6$). This implies the presence of short rod-like segments of native MWCNTs. The presence of such rod-like segments may be due to the comparatively high stiffness of MWCNTs. (iii) The high $q$ regime is characterized by a slope of $\alpha \cong -2$ for both MWCNTs and MWCNT-PS-1d, similar to the case of SWCNTs. Also, the SAXS curves exhibit the power-law behavior with $\alpha \cong -2$ to $-3$ (Figure 1f). However, for the sample MWCNT-PS-3d dispersed in D-toluene, significant excess scattering in the high $q$ range ($q$ > 0.02 Å$^{-1}$) is observed in SANS (Figure 1b). This implies the presence of a large amount of protonated PS grafts, which gives rise to incoherent scattering and results in the upshift of the background.

The scattering profiles of MWCNTs and MWCNT-PS-3d in HD-toluene are very similar to the ones of the corresponding SWCNTs (Figure 1c), exhibiting forward scattering with $\alpha \cong -4$ and an intermediate regime with $\alpha \cong -2$. Again, the profile of MWCNT-PS-3d is very similar to the one of MWCNT.
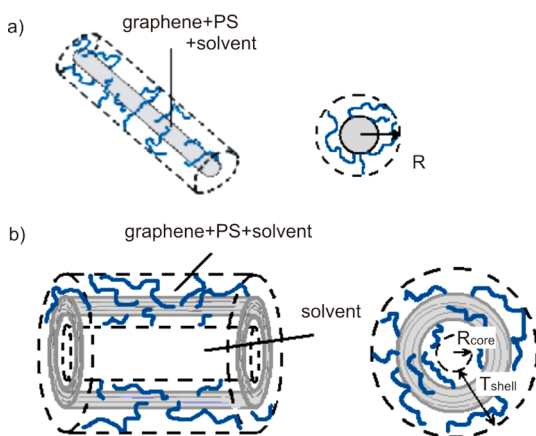
The overall character of the scattering profiles for the CNTs dispersions is similar to the scattering from the polysaccharide gels studied by Middendorf et al.[31,32] They were found to match the curves obtained from simulations of gel-like structures consisting of rod-like substructures. Therefore, the present system of dispersed CNTs in toluene can be approximated as a fractal organization of rod-like segments. Similar approximations were applied for the dispersions of CNTs in the polymer matrix as discussed in the Introduction.[24,25]

**Modeling of SAXS and SANS Curves.** In this section, the analytical models used for the interpretation of the scattering curves are discussed. In general, the dependence of the scattering intensity $I$ on the magnitude of the scattering vector $q$ is expressed as

$$I(q) = P(q)S(q) + bkg \tag{1}$$

where $P(q)$ is the single-particle form factor, depending on the shape and size of the scatterers, and $S(q)$ is the interparticle structure factor. $bkg$ denotes the background. Expressions for $P(q)$ and $S(q)$ are deduced from beforehand knowledge on the CNTs.

**Scheme 1. (a) Homogeneous Cylinder Model for the Modified SWCNTs and (b) Core-Shell Cylinder Model for the Modified MWCNTs**



A single CNT with its high aspect ratio, which can be as large as 1000, resembles a very thin and long cylinder. However, in practice, defects in the graphene structure of the CNTs' framework, such as the inclusion of five- or seven-membered rings within the carbon network, $sp^3$-hybridized defects with −H, −OH, −COOH, and other groups, kinks, and twists, lead to a significant flexibility of the cylinders.[33] Therefore, CNTs can be considered to be straight (i.e., stiff) only on small length scales. To approximate their arrangement in agglomerates, we describe them as short stiff cylinders which form fractals characterized by the length of the CNTs between the cross-points $L$ (i.e., the mesh size), the fractal dimension $D$, and the correlation length $\xi$, i.e., the agglomerate size. The fractal-structure factor used by us was derived by Teixeira[34]

$$S(q) = 1 + \frac{D \exp[\Gamma(D-1) \sin(D-1) \tan^{-1}(q\xi)]}{(qL)^D [1 + (q\xi)^{-2}]^{(D-1)/2}} \tag{2}$$

where $\Gamma(x)$ is the gamma function.

The different structures of SW and MWCNTs suggest a different description of the cylinder-like segments. SWCNTs are usually considered as cylinders formed by rolling up of a single graphene sheet. Because their diameters (7−25 Å) are small compared to the resolution of the scattering experiments, their hollow structure does not need to be taken into account and they can be considered as homogeneous cylinders having a mean radius $R$ and a mean length $L$ (Scheme 1a). The following form factor for randomly oriented homogeneous cylinders was used[35]

$$P_{\text{homcyl}}(q) = \frac{v_0}{V_{\text{cyl}}} \int_0^{\pi/2} \sin \theta \, d\theta$$

$$\left[ 2V_{\text{cyl}}(\eta_{\text{cyl}} - \eta_{\text{solv}}) \frac{\sin\left(\frac{qL \cos \theta}{2}\right)}{\frac{qL \cos \theta}{2}} \frac{J_1(qR \sin \theta)}{qR \sin \theta} \right]^2 \tag{3}$$

where $v_0$ is a scaling factor related to the volume fraction of the scatterers, $\eta_{\text{cyl}}$ and $\eta_{\text{solv}}$ are the SLDs of the cylinder and the solvent, respectively, and $J_1(x)$ the first order Bessel function. $\theta$ denotes the angle between the cylinder axis and the scattering vector, $\vec{q}$. The form factor $P_{\text{homcyl}}(q)$ is normalized by the particle volume, $V_{\text{cyl}}$, which is averaged over the normalized size distribution. The polydispersity of the cylinder radius was taken into account by a Schulz distribution

$$f(R) = (z + 1)^{z+1} x^z \frac{\exp[-(z + 1)x]}{\langle R \rangle \Gamma(z + 1)} \tag{4}$$

where $\langle R \rangle$ is the mean radius, $x = R/\langle R \rangle$, and $z$ is related to the polydispersity $p$ by $z = 1/p^2 - 1$.

The SLD of the cylinder, $\eta_{\text{cyl}}$, is the average of the SLD of the graphene layer and of the solvent inside the SWCNT, weighted by their volume fractions. The modified SWCNTs comprise an additional layer consisting of grafted PS and solvent (Scheme 1a), resulting in a different SLD. Since neither the exact structure of the SWCNTs nor the grafting density and length of the polymer chains are known, $\eta_{cyl}$ was used as a fitting parameter, and its value will be discussed in detail below. $\eta_{\text{solv}}$ was fixed in the fits at the values of D-toluene or HD-toluene, respectively.

In contrast to SWCNTs, MWCNTs typically have a much larger inner diameter of ~40 Å and a complex shell, consisting of several graphene layers with solvent in-between, which together results in a thickness of 100−160 Å. They were thus described using a core−shell cylinder model with the core of radius $R_{\text{core}}$ comprising the solvent. In case of native MWCNTs, the shell of thickness $T_{\text{shell}}$ consists of the graphene layers and of the solvent in-between; for modified MWCNTs, the solvent-swollen layer of PS is included in the shell as well (Scheme 1b). The form-factor used reads[35]

$$P_{\text{cosh cyl}}(q) = \frac{v_0}{V_{\text{core}}} \sum_{R_{\text{core}}} n(R_{\text{core}}, \sigma)$$

$$\int_0^{\pi/2} \sin\theta \, d\theta \left[ V_l(\eta_{\text{shell}} - \eta_{\text{solv}}) \frac{\sin\left(\frac{qL\cos\theta}{2}\right)}{\frac{qL\cos\theta}{2}} \right.$$

$$\frac{2J_1(qR_l\sin\theta)}{qR_l\sin\theta} + V_{\text{core}}(\eta_{\text{solv}} - \eta_{\text{shell}}) \frac{\sin\left(\frac{qL\cos\theta}{2}\right)}{\frac{qL\cos\theta}{2}}$$

$$\left. \frac{2J_1(qR_{\text{core}}\sin\theta)}{qR_{\text{core}}\sin\theta} \right]^2$$

$$(5)$$

where $V_x = \pi R_x^2 L$, $(x = l, \text{core})$. $R_l$ denotes the total cylinder radius ($R_l = R_{\text{core}} + T_{\text{shell}}$) and $\eta_{\text{shell}}$ the SLD of the shell. $\sigma$ is the standard deviation of the log-normal distribution. $v_0$ is the volume fraction of the cylinders. The normalized log-normal distribution takes into account the polydispersity of the core radius

$$n(R_{\text{core}}, \sigma) = \frac{\exp\left(-\frac{1}{2}\left[\frac{\ln(R_{\text{core}}/\langle R_{\text{core}}\rangle)}{\sigma}\right]^2\right)}{\sqrt{2\pi}\,\sigma R_{\text{core}}}$$

$$(6)$$

Here, $\langle R_{\text{core}}\rangle$ is the mean value of the distribution of $R_{\text{core}}$. Using the SLD of the solvent in eq 5 takes into account that the core of the cylindrical particles is filled with solvent. As in the case of SWCNTs, $\eta_{\text{shell}}$ is a fitting parameter. Again, the SLD of the surrounding solvent, $\eta_{\text{solv}}$, was fixed in the fits at the values of D-toluene or HD-toluene, respectively.

Hereafter, the two models will be abbreviated as "Polydisperse homogeneous cylinder/Fractal" and "Polydisperse core-shell cylinder/Fractal". All fits were carried out using the package "SANS & USANS Analysis with IGOR Pro" written at the NIST Center for Neutron Research (Gaithersburg, U.S.A.).[36]

**Results from Modeling.** The SANS data cover quite a large range of $q$ values, thus giving information on both the long-range correlation and on the small-scale features of the system. However, the results unavoidably suffer from large uncertainties, due to two factors: (i) Despite the long accumulation times, the statistics is poor because of the low concentration of the scatterers in the dispersions: The concentration of CNTs was 0.5 or 1.0 mg/mL, corresponding to a volume fraction of the scatterers of ca. 0.003 or 0.006 (assuming a bulk density of CNTs of ca. 0.15 g/cm³). This is especially pronounced for the dispersions of CNTs in D-toluene, where the signal is mainly due to the grafted PS chains which have an even lower volume fraction. (ii) The broad distribution of the CNTs' dimensions results in large uncertainties. To get a consistent set of parameters from SAXS and SANS, the large scale parameters, like the length of the cylinders, correlation length and fractal dimensions, were fixed during the analysis of the SAXS curves, whereas small scale parameters, namely the core radius were in some cases fixed during the analysis of the SANS curves.

The SANS curves together with the fits are depicted in Figure 3. The simple model fits all curves well over the entire $q$ range, in spite of the complex structure of the CNTs and their
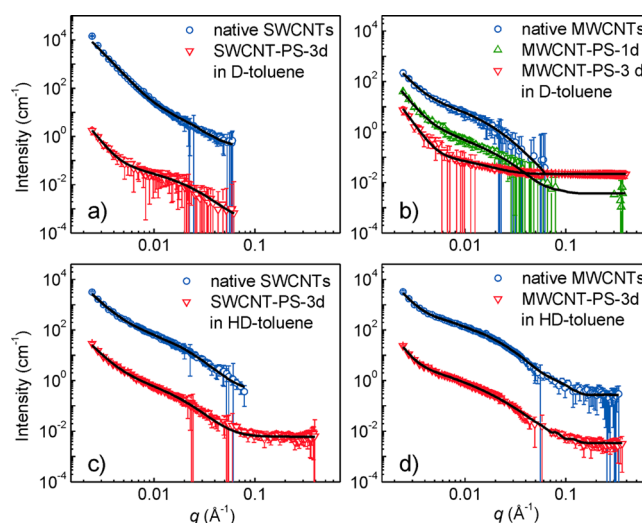


**Figure 3.** Fits to the experimental SANS curves in D-toluene (a and b) and in HD-toluene (c and d), all at 0.5 mg/mL. Lines: model fits (eqs 1−6, see text). For clarity, the curves of the native CNTs were shifted upward by a factor of 100 and the ones of SW(MW)CNT-PS-1d by a factor of 10.

clusters. The fitting parameters are given in Figure 4 and in Tables 2 and 3.

In all SANS curves, forward scattering is present, i.e., a certain fraction of the CNTs form agglomerates. Our expectation was that, with increasing amount of PS, the aggregates would be more loosely packed, resulting in a reduced fractal dimension $D$. Moreover, we expected the aggregate size, i.e., the correlation length $\xi$ in eq 2 to decrease with increasing amount of grafted polymer. However, from the fits, $D$ was found to be close to 3 in all cases, and $\xi$ remained at ca. $10^4$–$10^5$ Å (not shown). This means that regardless of the amount of grafted PS, (i) the CNTs stay agglomerated in the toluene dispersion, (ii) their packing in the agglomerate remains a three-dimensional network of rod-like segments, and (iii) the agglomerate size remains unchanged.

Nevertheless, on smaller length scales, the modification of the SW and MWCNTs does affect their dispersion ability. The length of the cylindrical segments, $L$, increases from ca. 500 to ca. 5800 Å for SWCNTs (Figure 4a) and from ca. 830 to ca. 8000 Å for MWCNTs (Figure 4c) with the amount of grafted polymer, i.e. the mesh size in the agglomerates increases by more than a factor of 10, which means that the agglomerates formed by the PS-modified CNTs are much more loosely packed than the ones formed by the native ones.

The measurements of the MWCNTs in HD-toluene, where the bare MWCNTs are highlighted and PS is not expected to be observable, show that all radii are unaffected by the modification: $R_{\text{core}} \cong 17$ Å, $T_{\text{shell}} \cong 34$–$36$ Å, and $R_l \cong 50$–$54$ Å (Figure 4b,d). Within the uncertainties, $R_{\text{core}}$ stays constant at ca. 17 Å. In contrast, in D-toluene, where the PS-grafts of the MWCNTs are highlighted, changes in $R_{\text{core}}$ and $T_{\text{shell}}$ are observed: For MWCNT-PS-3d, $T_{\text{shell}}$ is with 58 Å larger than for the native MWCNTs (43 Å) (Figure 4d). However, for MWCNT-PS-1d, $T_{\text{shell}}$ is unchanged from the native MWCNTs. This may indicate that (i) the short polymer chains obtained after 1 day are wrapped around the CNTs and/or (ii) the modified CNTs are exfoliated to a higher degree.

Interestingly, for the MWCNTs in D-toluene, $R_{\text{core}}$ decreases from 22 Å for native MWCNTs to 12 Å for MWCNT-PS-1d
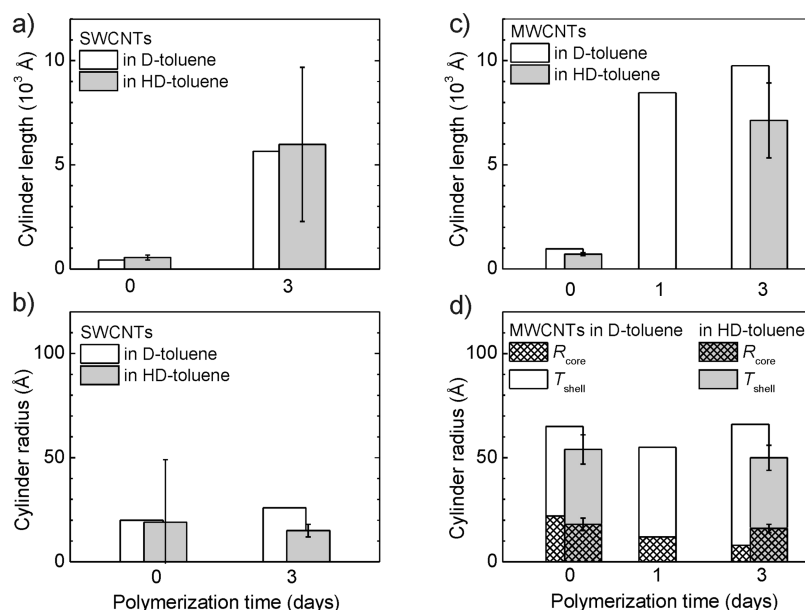
**Figure 4.** Results on cylinder dimensions from SANS at 0.5 mg/mL in dependence on polymerization time. Length $L$ (a and c) of the SWCNTs (a) and MWCNTs (c). Cylinder radius $R$ of the SWCNTs (b). Core radius, $R_{core}$, and shell thickness, $T_{shell}$, of the MWCNTs (d).

**Table 2. SLDs of the SWCNTs Using the Polydisperse Homogeneous Cylinder/Fractal Model on SANS at 0.5 mg/mL**

|  | $\eta_{cyl}$ ($10^{-6}$ Å$^{-2}$) | |
| --- | --- | --- |
| sample | in D-toluene | in HD-toluene |
| SWCNT | 5.52 | 2.20 ± 0.03 |
| SWCNT-PS-3d | 5.42 | 2.20 ± 0.03 |

**Table 3. SLDs of the Shells of the MWCNTs Using the Polydisperse Core-Shell Cylinder/Fractal Model on SANS at 0.5 mg/mL**

|  | $\eta_{shell}$ ($10^{-6}$ Å$^{-2}$) | |
| --- | --- | --- |
| sample | in D-toluene | in HD-toluene |
| MWCNT | 5.39 | 2.74 ± 0.09 |
| MWCNT-PS-1d | 5.29 | a |
| MWCNT-PS-3d | 5.24 | 2.72 ± 0.13 |

$^a$Not measured.

and to 8 Å for MWCNT-PS-3d (Figure 4d). This indicates the presence of PS grafts not only on the outer walls of the CNTs but on the inner ones as well. The result is consistent with our observation on intercalative growth of polymer chains on CNTs made on the base of Raman spectroscopy and TGA analysis.[18]

From the comparison of the shell thicknesses of native and modified MWCNTs (Figure 4d), which comprise the graphene layers alone and the graphene layers together with the PS shell, respectively, we conclude that the thickness of the PS shell is, on average, below 12 Å.

In the SWCNT dispersions in D-toluene, where PS is highlighted, the radii of the dispersed SWCNTs increase slightly from $R \cong 20$ Å for native SWCNTs to 26 Å for SWCNT-PS-3d (Figure 4b). The value of 20 Å is significantly larger than specified for single SWCNTs (diameters of 7−25 Å according to the manufacturer); that is, ropes consisting of several SWCNTs are present. Upon grafting PS, the SWCNTs' radius increases due to the PS grafts; however, the dispersibility

of the SWCNTs increases as well. Thus, the modified SWCNTs are more easily exfoliated from the ropes existing in the native samples, and the ropes consist of fewer tubes. Hence, the average radius is nearly unchanged upon modification. The SANS experiments in HD-toluene, where the bare CNTs are highlighted, confirm this idea: $R$ decreases from ca. 18 Å for the native SWCNTs to ca. 14 Å for the SWCNTs-PS-3d (Figure 4b).

The SLDs (Tables 2 and 3) contain information on the composition of the cylinders. The models comprise homogeneous and constant SLDs of the cylindrical segments in the case of SWCNTs or within the core and the shell in MWCNTs. However, real CNTs have a hollow-core structure with one angstrom (for SWCNTs) or several angstroms (for MWCNTs) thick graphene walls with an interlayer distance of ca. 3.4 Å in-between.[37,38] The modified CNTs are decorated with PS grafts, which are presumably inhomogeneously distributed along the tubes (Scheme 1). Furthermore, intercalative grafting of PS is expected, resulting in the presence of PS in-between the graphene layers and inside the tubes.[18] Moreover, solvent enters the space between the graphene layers and between the PS grafts. Thus, the cylindrical segments represent a three-component system of graphene, solvent and PS. Neglecting the inhomogeneities within the individual phases, the average SLD of each domain reads

$$\langle \eta \rangle = \sum_{i=1}^{n} \eta_i \varphi_i \qquad (7)$$

with $\eta_i (i = 1 ..., n)$ being the SLDs of the components present in the domains having each a volume fraction $\varphi_i$ with $\sum_{i=1}^{n} \varphi_i = 1$. The SLDs of the shell (for MWCNTs) or of the homogeneous cylinder (for SWCNTs) are thus expressed as follows:

$$\eta_{shell/cyl} = \eta_{graphene}\varphi_{graphene} + \eta_{PS}\varphi_{PS} + \eta_{solvent}$$
$$[1 - (\varphi_{graphene} + \varphi_{PS})] \qquad (8)$$

For the dispersions of CNTs in HD-toluene, the SLD of PS is matched by the solvent; that is, the SLD can be approximated as an average of only two components, graphene and solvent

$$\eta_{shell/cyl} = \eta_{graphene}\varphi_{graphene} + \eta_{HD-tolune}[1 - \varphi_{graphene}] \quad (9)$$

The average volume fraction of PS reads $\varphi_{PS} = \alpha\varphi_{graphene}$. $\alpha$ is deduced from the weight fraction values $w$ known from TGA (Table 1)

$$\alpha = \frac{V_{PS}}{V_{PS} + V_{graphene}}$$

$$= \frac{1}{1 + \dfrac{m_{graphene}}{m_{PS}}\dfrac{\rho_{PS}}{\rho_{graphene}}}$$

$$= \frac{1}{1 + \left(\dfrac{1}{w} - 1\right)\dfrac{\rho_{PS}}{\rho_{graphene}}} \quad (10)$$

$\rho_{graphene}$ and $\rho_{PS}$ are the solid density of the CNTs and the mass density of PS, respectively. $m_{graphene}$ and $m_{PS}$ are the masses of graphene and PS, respectively. The resulting $\alpha$ values for SW and MWCNTs having different amounts of PS are given in Table 4.

**Table 4. Weight and Volume Fractions of PS with Respect to Graphene**

| sample | $w^a$ | $\alpha$ |
|---|---|---|
| SWCNT-PS-1d | 0.10 | 0.14 |
| SWCNT-PS-3d | 0.18 | 0.25 |
| MWCNT-PS-1d | 0.16 | 0.20 |
| MWCNT-PS-3d | 0.32 | 0.38 |

[a]From TGA.[18]

**Table 5. Thickness of the Graphene Layer in the CNTs from the SANS Fitting Parameters of the Dispersions in D-Toluene at 0.5 mg/mL**

| sample | $\eta_{shell,}$ $\eta_{cyl}^{a}$ $(10^{-6}$ Å$^{-2})$ | $\alpha^b$ | $\varphi_{graphene}^{b}$ | thickness of shell/cylinder$^a$ (Å) | thickness of graphene layer$^c$ (Å) |
|---|---|---|---|---|---|
| SWCNT | 5.52 | 0 | 0.21 | 20 | 4.2 |
| SWCNT-PS-3d | 5.42 | 0.25 | 0.14 | 26 | 3.6 |
| MWCNT | 5.39 | 0 | 0.28 | 43 | 12.0 |
| MWCNT-PS-1d | 5.29 | 0.20 | 0.21 | 43 | 8.8 |
| MWCNT-PS-3d | 5.24 | 0.38 | 0.16 | 58 | 9.5 |

[a]From SANS. [b]From TGA. [c]For MWCNTs and SWCNTs, the graphene SLD values of $4.7 \times 10^{-6}$ and $5 \times 10^{-6}$ Å$^{-2}$ were used, which are based on the solid densities.

From $\eta_{shell}$, $\eta_{cyl}$, $R$ and $T_{shell}$ from SANS together with $\alpha$ from TGA, eqs 8 and 9 provide the volume fraction of the graphene layers in the cylindrical segments, and thus, their thicknesses. They are consistently found at 3–5 Å and 8–15 Å for the SWCNTs and the shells of the MWCNTs, respectively (Tables 5 and 6).

In order to estimate the number of the walls present in the MWCNTs and the number of SWCNTS forming the ropes, knowledge of the thickness of a single graphene layer in CNTs is required. Despite of a number of theoretical calculations of

**Table 6. Thickness of Graphene Layer in the CNTs from the SANS Fitting Parameters for Dispersions in HD-Toluene at 0.5 mg/mL**

| sample | $\eta_{shell,}$ $\eta_{cyl}^{a}$ $(10^{-6}$ Å$^{-2})$ | $\varphi_{graphene}^{b}$ | thickness of shell/cylinder$^a$ (Å) | thickness of graphene layer$^c$ (Å) |
|---|---|---|---|---|
| SWCNT | 2.20 | 0.22 | 19 | 4.2 |
| SWCNT-PS-3d | 2.20 | 0.22 | 14 | 3.1 |
| MWCNT | 2.74 | 0.41 | 36 | 14.8 |
| MWCNT-PS-3d | 2.72 | 0.40 | 34 | 13.6 |

[a]From SANS. [b]From TGA. [c]For MWCNTs and SWCNTS, the graphene SLD values of $4.7 \times 10^{-6}$ Å$^{-2}$ and $5 \times 10^{-6}$ Å$^{-2}$ were used.
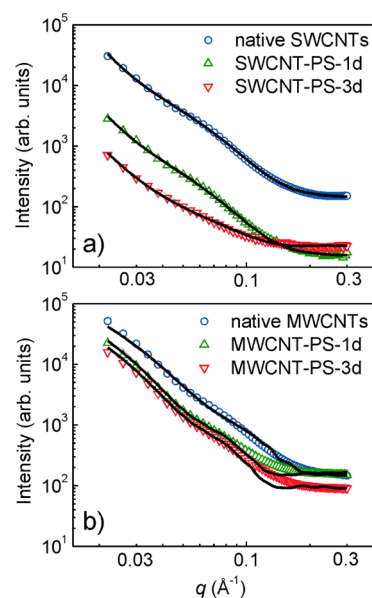


**Figure 5.** Fits of the experimental SAXS curves of 1 mg/mL dispersions of (a) SW and (b) MWCNTs in H-toluene. Lines: model fits (eqs 1−6, see text).

**Table 7. Fitting Parameters of the SAXS Curves SAXS Curves of SWCNTs at 1 mg/mL Using the Polydisperse Homogeneous Cylinder/Fractal Model**

| sample | $R$ (Å) | $L$ (Å) | $\eta_{cyl}^{a}$ $(10^{-6}$ Å$^{-2})$ |
|---|---|---|---|
| SWCNT | 14.6 | 617 | 9.5 |
| SWCNT-PS-1d | 16 | 4860 | 9.02 |
| SWCNT-PS-3d | 23 | 5690 | 8.86 |

[a]$\eta_{solv}$ was fixed at $8 \times 10^{-6}$ Å$^{-2}$.

**Table 8. Fitting Parameters of the SAXS Curves of MWCNTs at 1 mg/mL Using the Polydisperse Core-Shell Cylinder Model**

| sample | $R_{core}$ (Å) | $T_{shell}$ (Å) | $L$ (Å) | $\eta_{shell}^{a}$ $(10^{-6}$ Å$^{-2})$ |
|---|---|---|---|---|
| MWCNT | 18 | 30 | 700 | 9.55 |
| MWCNT-PS-1d | 19 | 42 | 9010 | 9.08 |
| MWCNT-PS-3d | 19.5 | 42 | 8900 | 8.96 |

[a]$\eta_{solv}$ was fixed at $8 \times 10^{-6}$ Å$^{-2}$.

the CNT wall thickness, there is no consensus on the exact value. Some theoretical calculations suggest the wall thickness to be equal to the graphite interlayer spacing (3.4 Å)[37] or to the bond length of the C═C double bond in the CNTs
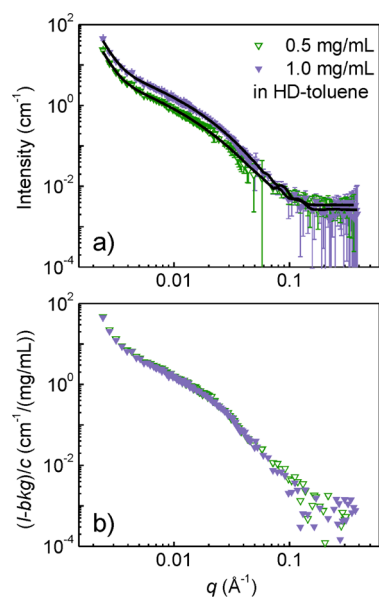
**Figure 6.** SANS curves of MWCNT-PS-3d dispersed in HD toluene. (a) 0.5 mg/mL (lower curve) and 1 mg/mL (upper curve). Lines: model fits, see text. (b) Same curves normalized by the concentration $c$ of the CNTs.

structure.[38] In the model of Cai et al.,[39] the wall thickness is defined as the "thickness" of the electron cloud of an SWCNT and is with ca. 3.2 Å slightly larger than twice the C−C single bond length (2.824 Å). However, much smaller values have been reported as well: For instance, values in the range of 0.6−0.9 Å have been found in atomistic simulations and continuum shell models,[40] and energy equivalence between molecular and structural mechanics leads to a wall thickness of 1.47 Å.[41] A similar uncertainty concerns the interlayer distance between the walls. Usually, it is considered to be constant at 3.4 Å, which is 3−5% larger than that of the graphite-layer spacing.[3,42] However, Kiang et al. pointed out that the spacing between the graphene layers may depend both on the curvature and the number of layers, thus ranging from 3.42 to 3.75 Å.[43]

Taking the mean value of 1.0−1.5 Å for the wall thickness and 3.4 Å for the interlayer distance, the value of $T_{shell}$ from SANS in HD-toluene (34−36 Å, Figure 4d) is reproduced (31.8−35.8 Å) if the number of walls is assumed to be 8. This is consistent with the mean value of the wall number (3−15) given by the manufacturer. Moreover, the calculated graphene thickness of the order of 8−15 Å corresponds to MWCNTs composed of 8−10 walls. For the SWCNTs, we find values of 3−5 Å for the graphene thickness which means that the ropes consist of 2−4 CNTs.

The models suggested for SW and MWCNTs fit the SAXS data relatively well (Figure 5, Tables 7 and 8). However, for the MWCNT systems, there are deviations of the modeled curves from the experimental values at high $q$ values, probably because the model is too simple to describe the small-scale features.

Though the length of the cylindrical segments cannot be resolved within this $q$ range, the overall tendency of the scattering profile gives values which are in good agreement with the SANS results.

It should be noted that SAXS was performed on dispersions of CNTs with the concentration 1 mg/mL, while 0.5 mg/mL was used for SANS. To verify whether the dispersion ability of the CNTs is affected, SANS curves of MWCNT-PS-3d dispersions in HD-toluene were measured at 0.5 and 1 mg/mL (Figure 6a) on an absolute scale. The resulting fitting parameters are almost identical (Table 9), except for the scale which depends on the concentration of scatterers, $c$. The experimental data, when plotted as $(I − bkg)/c$ vs $q$, lie on top of each other (Figure 6b). Thus, within the uncertainties, the parameters obtained from SAXS and SANS at the two concentrations are expected to be unaffected by the concentration itself. Deviations of the fitting curves from the experimental data can be explained by the complexity and the high polydispersity of the real system.

## ■ CONCLUSIONS

SIPGP was successful in modifying CNTs with PS. Small-angle neutron and X-ray scattering (SANS/SAXS) experiments on dispersions of CNTs in toluene allowed for studying of the influence of this modification on both their morphology and aggregation behavior. Despite the high polydispersity of the system and the complex structure of the CNTs, the model system of homogeneous or core−shell cylinders for SW and MWCNTs, respectively, forming large agglomerates fits the experimental curves well. The improved dispersion ability upon modification of the CNTs with polymer grafts is reflected in an increase of the mesh size by a factor of ca. 10 to ca. 7000−9000 Å. SWCNTs most probably form ropes consisting of 2−4 tubes. Alteration of the solvent (D-toluene or HD-toluene) in SANS experiments allowed us a detailed characterization of the shell formed by PS grafts: Grafting occurs not only on the outer walls of the CNTs, but, in case of MWCNTs, on the inner tubes as well. The thickness of the PS shell is lower than ca. 12 Å.

The presented study is one of the very few investigations of the dispersion behavior of CNTs in a liquid phase (solvent) and its dependence on the modification of the CNTs: Most of the previous works, as discussed in the Introduction, concern the study of distribution of CNTs in a solid phase, e.g., a polymer matrix. The characterization of CNTs in a solvent allows studying both their dispersion ability and the morphological changes of the CNTs upon modification with polymer grafts. The latter is not possible when the CNTs are already introduced in a polymer matrix. Also, the characterization of the dispersion ability of CNTs in solvents as a function of their modification level is of great importance for the optimization of the solution processing for preparation of CNTs/polymer nanocomposites.

**Table 9. Fitting Parameters of the SANS Curves of MWCNT-PS-3d with Concentrations 0.5 and 1 mg/mL Using the Polydisperse Core-Shell Cylinder/Fractal Model**

| concentration (mg/mL) | scale | $R_{core}$ (Å) | $T_{shell}$ (Å) | $L$ (Å) | $\eta_{shell}$[a] ($10^{-6}$ Å$^{-2}$) |
|---|---|---|---|---|---|
| 0.5 | 0.003 | 15.8 ± 2.4 | 34.1 ± 3.9 | 7100 ± 1900 | 2.72 |
| 1.0 | 0.006 | 15.0 ± 1.6 | 35.0 ± 2.5 | 6900 ± 960 | 2.70 |

$^a\eta_{solv}$ was fixed at $1.40 \times 10^{-6}$ Å$^{-2}$

## ■ AUTHOR INFORMATION

### Notes

The authors declare no competing financial interest.

## ■ ACKNOWLEDGMENTS

## ■ REFERENCES

(1) Szleifera, I.; Yerushalmi-Rozen, R. *Polymer* **2005**, *46*, 7803.

(2) Radushkevich, L. V.; Lukyanovich, V. M. *J. Phys. Chem. Russia* **1952**, *1*, 88.

(3) Iijima, S. *Nature* **1991**, *354*, 56.

(4) Safarova, K.; Dvorak, A.; Kubinek, R.; Vujtek, M.; Rek, A. *Mod. Res. Ed. Top. Microsc.* **2007**, *2*, 513.

(5) Bellucci, S.; Gaggiotti, G.; Marchetti, M.; Micciulla, F.; Mucciato, R.; Regi, M. *J. Phys.: Conf. Ser.* **2007**, *61*, 99.

(6) Kim, J.; Xiong, H.; Hofmann, M.; Kong, J.; Amemiya, S. *Anal. Chem.* **2010**, *82*, 1605.

(7) Backes, C.; Englert, J. M.; Bernhard, N.; Hauke, F.; Hirsch, A. *Small* **2010**, *6*, 1968.

(8) Moniruzzaman, M.; Winey, K. I. *Macromolecules* **2006**, *39*, 5194.

(9) Coleman, J. N.; Khan, U.; Blau, W. J.; Gun'ko, Y. K. *Carbon* **2006**, *44*, 1624.

(10) Pujari, S.; Ramanathan, T.; Kasimatis, K.; Masuda, J.; Andrews, R.; Torkelson, J. M.; Brinson, L. C.; Burghardt, W. R. *J. Polym. Sci B: Polym. Phys.* **2009**, *47*, 1426.

(11) Schaefer, D. W.; Zhao, J.; Brown, J. M.; Anderson, D. P.; Tomlin, D. W. *Chem. Phys. Lett.* **2003**, *375*, 369.

(12) Song, Y. S.; Youn, J. R. *Carbon* **2005**, *43*, 1378.

(13) Sahooa, N. G.; Ranab, S.; Chob, J. W.; Li, L.; Chana, S. H. *Prog. Polym. Sci.* **2010**, *35*, 837.

(14) Tang, Q. Y.; Shafiq, I.; Chan, Y. C.; Wong, N. B.; Cheung, R. *J. Nanosci. Nanotechnol.* **2010**, *10*, 4967.

(15) Ding, W.; Eitan, A.; Fisher, F. T.; Chen, X.; Dikin, D. A.; Andrews, R.; Brinson, L. C.; Schadler, L. S.; Rudf, R. S. *Nano Lett.* **2003**, *3*, 1593.

(16) Lourie, O.; Wagner, H. D. *Appl. Phys. Lett.* **1998**, *73*, 3527.

(17) Ajayan, P. M.; Schadler, L. S.; Giannaris, C.; Rubio, A. *Adv. Mater.* **2000**, *12*, 750.

(18) Golosova, A.; Mendrek, A.; Steenackers, M.; Schulte, L.; Ndoni, S.; Papadakis, C. M.; Jordan, R. to be published.

(19) Steenackers, M.; Küller, A.; Stoycheva, S.; Grunze, M.; Jordan, R. *Langmuir* **2009**, *25*, 2225.

(20) Bauer, B. J.; Hobbie, E. K.; Becker, M. L. *Macromolecules* **2006**, *39*, 2637.

(21) Zhou, W.; Islam, M. F.; Wang, H.; Ho, D. L.; Yodh, A. G.; Winey, K. I.; Fischer, J. E. *Chem. Phys. Lett.* **2004**, *384*, 185.

(22) Urbina, A.; Miguel, C.; Delgado, J. L.; Langa, F.; Díaz-Paniagua, C.; Batallán, F. *Phys. Rev. B* **2000**, *78*, 045420.

(23) Roe, R. J. *Methods of X-Ray and Neutron Scattering in Polymer Science*; Oxford University Press: Oxford, U.K., 2000.

(24) Zhao, C.; Hu, G.; Justice, R.; Schaefer, D. W.; Zhang, S.; Yang, M.; Han, C. C. *Polymer* **2005**, *46*, 5125.

(25) Justice, R. S.; Wang, D. H.; Tan, L.-S.; Schaefer, D. W. *J. Appl. Crystallogr.* **2007**, *40*, 88.

(26) NIST, Scattering length density calculator, http://www.ncnr.nist.gov/resources/sldcalc.html.

(27) Lindner, P.; May, R. P.; Timmins, P. A. *Physica B* **1992**, *180*, 967.

(28) Lindner, P.; Schweins, R. *Neutron News* **2010**, *21−2*, 15.

(29) NIST, Scattering length density calculator, http://www.ncnr.nist.gov/resources/sldcalc.html.

(30) Lindner, P. In *Neutrons, X-Rays and Light: Scattering Methods Applied to Soft Condensed Matter*; Lindner, P., Zemb, Th., Eds.; Elsevier−North Holland Delta Series: Amsterdam, 2002; Chapter 2.

(31) Deriu, A.; Cavatorta, E.; Di Cola, D.; Middendorf, H. D. *J. Phys. IV Coll. C1, J. Phys. II (suppl)* **1993**, *3*, 237.

(32) Middendorf, H. D.; Hotz de Baar, O. F. A. *J. Mol. Struct.* **1996**, *383*, 241.

(33) Hirsch, A. *Angew. Chem., Int. Ed.* **2002**, *41*, 1853.

(34) Teixeira, J. *J. Appl. Crystallogr.* **1988**, *21*, 781.

(35) Guinier, A.; Fournet, G. *Small-Angle Scattering of X-Rays*; John Wiley and Sons: New York, 1955.

(36) Kline, S. *J. Appl. Crystallogr.* **2006**, *39*, 895.

(37) Lu, J. P. *Phys. Rev. Lett.* **1997**, *79*, 1297.

(38) Cai, J.; Bie, R. F.; Tan, X. M.; Lu, C. *Physica B* **2004**, *344*, 99.

(39) Cai, J.; Wang, C. Y.; Yu, T.; Yu, S. *Phys. Scr.* **2009**, *79*, 025702.

(40) Huang, Y.; Wu, J.; Hwang, K. C. *Phys. Rev. B* **2006**, *74*, 245413.

(41) Tserpesa, K. I.; Papanikos, P. *Composites: Part B* **2005**, *36*, 468.

(42) Ebbesen, T. W.; Ajayan, P. M. *Nature* **1992**, *358*, 220.

(43) Kiang, C. H.; Endo, M.; Ajayan, P. M.; Dresselhaus, G.; Dresselhaus, M. S. *Phys. Rev. Lett.* **1998**, *81*, 1869.